CHAPTER 8

Time-Resolved X-ray Absorption Spectroscopy Methods

T. Ressler[1], J. A. van Bokhoven[2], G. Knop-Gericke[1], F. M. F. de Groot[3]

[1]Fritz-Haber-Institut der MPG, Department of Inorganic Chemistry, Faradayweg 4-6, 14195 Berlin, Germany

[2]Laboratory for Technical Chemistry, ETH Hönggerberg, CH-8093 Zurich, Switzerland

[3]Department of Inorganic Chemistry and Catalysis, Utrecht University, Sorbonnelaan 16, 3508 TB Utrecht, The Netherlands

CONTENTS

1. INTRODUCTION

X-ray absorption spectroscopy (XAS) is a powerful technique that provides element-specific short-range structural information. XAS probes the local order and, hence, can be applied to structurally disordered and ordered solids, and to dispersed species (e.g., small metal cluster). X-ray absorption spectroscopy in the hard X-ray regime ($>$ 2.5 keV) can be performed *in-situ* under reaction conditions with pressures and temperatures larger than 1 bar and 293 K, respectively (see preceding chapters and references therein). A large number of elements from the Periodic Table, in particular, main group metals and transition metals, are accessible for *in-situ* XAS studies at photon energies higher than 2.5 keV. Therefore, XAS offers a high potential for the structure determination in heterogeneous catalysis complementary to many standard methods such as X-ray diffraction or Raman spectroscopy.

Because only a thin line separates *in-situ* XAS studies from time-resolved XAS investigations, in the following chapter, we focus on *in-situ* XAS investigations aiming, first, at understanding structural evolution under dynamic conditions and, second, at revealing properties of the system studied not available from investigations under stationary conditions. In the literature cited in this chapter, not only was the local structure of

ISBN: 0-00000-000-0/$25.00

In-situ Spectroscopy of Catalysts
Edited by H. S. Nalwa

a material studied under reaction conditions, but also were characteristic properties of the reaction elucidated, such as reaction intermediates or the kinetics of the reaction. This distinguishes the investigations described in this chapter from *in-situ* structural investigations under stationary conditions.

The reactivity of solids and the kinetics of solid-state reactions constitute important subjects in heterogeneous catalysis research. In many cases, the active catalyst is obtained from a precursor phase, for instance, by thermal decomposition under different atmospheres, or by reduction with hydrogen or directly in the catalysis feed. Moreover, not only preparation and activation of a catalyst involve reactions of the catalyst bulk. Although most reactions in heterogeneous catalysis proceed on the surface of a catalytically active phase, this active phase and its surface may be influenced or even determined by the underlying catalyst bulk. Studies on the preparation procedure and the structure of a catalyst under dynamic conditions have in common that, not only the geometric and electronic structure of the individual phases involved are of interest, but also the transition of one phase into another, hence, the mechanism or the kinetics of this reaction. Naturally, structural evolution and kinetics of phase transitions can only be obtained from time-resolved *in-situ* studies. By using X-ray absorption spectroscopy in a time-resolved mode, investigations of the bulk structural response of a catalysis system to rapidly changing dynamic reaction conditions can be performed with a sub-second time-resolution and, thus, result in reliable structure-reactivity relationships.

Several recent publications have reviewed parts of the literature related to time-resolved XAS (TR-XAS) [1–5]. Time-resolved XAS studies in the different areas of chemistry, catalysis or material sciences have been performed for roughly one decade now. However, in particular, in the years 2001 and 2002, investigations employing TR-XAS appear to increase. Here, an overview of the existing TR-XAS literature is given. In addition, a number of points are emphasized that are, according to the authors, particularly important to time-resolved XAS investigations. The following section focuses on the characteristics of time-resolved (TR) *in-situ* XAS experiments and for the analysis of TR-XAS data with respect to elucidating the "real" structure of heterogeneous catalysts.

2. INSTRUMENTATION FOR TR-XAS

The majority of conventional XAS beamlines operating in the hard X-ray regime (> 2.5 keV) are dedicated to transmission and fluorescence EXAFS using a double crystal monochromator to monochromatize the radiation coming from a bending magnet or an insertion device. The wavelength and energy of the photons impinging on the sample are determined by the Bragg angle and the lattice plane distance of the monochromator material used. In the transmission mode, the absorption of the sample is measured with ionization chambers or photo diodes before (Io) and after (I1) the sample. Quite often, a reference compound located between the second and third detector is measured simultaneously. In order to obtain a reliable data quality in the step-scanning mode, a total measuring time of at least several minutes is required. In the QEXAFS (Quick-EXAFS) [6, 7] technique, the stepper motors of the monochromator crystals are driven continuously with a simultaneous read-out of the detectors. The measuring time is decreased to several tenths of a second. Channel-cut monochromators adjusted by piezo crystals can further reduce the measuring time by a factor of ∼ 100 [8]. A disadvantage of this approach is the restricted spectral range due to the finite translation of the piezo crystals. However, a number of recent developments promise a continuous increase in time-resolution available with the QEXAFS technique, with improved stability and data quality: new detectors [9], improved monochromator crystal bender [10] and QEXAFS at a third generation source [11]. Evidently, QEXAFS offers a superior versatility as experiments can be performed in different detection modes (transmission, fluorescence, electron yield, etc.) on a large variety of systems (solid, liquid or diluted samples, enhanced surface sensitivity, etc.). Furthermore, an increased number of reports can be found where TR-QEXAFS has been combined with other experimental techniques (see below).

Another spectrometer set-up that can be used for TR-XAS investigations is the energy-dispersive XAFS (DXAS [12]) technique. The first experiment combining dispersive optics and XAS was performed by Kaminaga et al. [13] in 1981 using a plane Si(111) monochromator in transmission geometry on an X-ray tube. It recorded the intensity distribution with a position-sensitive proportional counter. The measuring time for a single absorption spectrum amounted to several hours. Applying the advantages of synchrotron radiation, the necessary measuring time per spectrum has been decreased by several orders of magnitude. In the most common energy-dispersive set-up, the incoming synchrotron radiation is focused by a bent monochromator crystal in either reflection or transmission geometry (Figure 1). The curvature of the bend crystal results in a variation of the Bragg angle over the crystal surface, and, hence, to a defined position-energy correlation on the detector. The sample is located in the polychromatic focal point. With the energy-dispersive set-up, an entire absorption spectrum is collected at once, without requiring any movement of the spectrometer components. Therefore, a superior stability of the DXAS set-up permits reliable detection of small changes in the experimental spectra. The energy range available for EXAFS analysis is restricted by the Bragg angle used and, hence, by the edge energy of the absorber to be measured. Generally, at edge energies below ∼10 keV the energy range available using a Si(111) crystal, is not suffi-

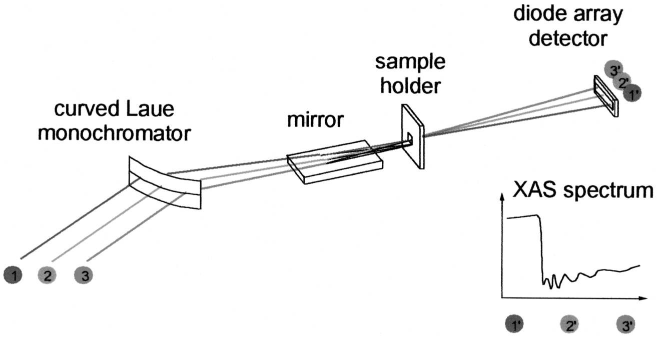

Figure 1. Schematic representation of an energy-dispersive XAS spectrometer. The characteristic elements of the beamline and the beam path are indicated.

cient for a detailed EXAFS analysis. Furthermore, DXAS studies are restricted to the transmission mode, which poses certain concentration limitations on the systems that can be investigated. This is important in combination with a heavily absorbing matrix. Although the energy-dispersive set-up poses higher demands on the homogeneity of samples studied, reliable EXAFS data of sufficient quality can be obtained in the DXAS mode with a time-resolution in the sub-second range (Figure 2). The photo diode arrays currently in use at some energy-dispersive XAS spectrometers offer a high dynamic range, but only a moderate minimum integration time due to the necessary read-out time after the exposure. Additionally, photo diode arrays suffer from radiation damage, as already mentioned above. For the dispersive XAS beamline at the ESRF (ID 24), a new detector design based on a scintillating screen lens-coupled to a CCD camera, was developed and has been successfully employed in numerous applications [14].

Recent developments of the energy-dispersive set-up have increased the usability of this technique for TR-XAS investigations. Energy-dispersive XAS experiments performed at photon energies of about 20 keV and using a Si(400) crystal in the Bragg geometry exhibit a strong reduction of sharp features in the XANES region of the measured absorption spectra and also a reduced amplitude in the EXAFS. Evidently, this loss of resolution is because of an asymmetric broadening of the reflectivity profile for a Bragg-type crystal. By applying a transmission-type monochromator (Laue geometry), a sufficiently resolved Pd K-edge (24.4 keV) absorption spectrum can be obtained [15].

Another effect frequently observed in dispersive XAS experiments with catalyst samples is a reduction of sharp features, e.g., 'white lines' or 'glitches', with increasing sample thickness. Although this effect is known for the standard XAS set-up as well (the thickness effect), a significant loss of intensity in the dispersive case can already be observed for sample thickness of several hundred microns and an absorption edge jump less than 0.5. The origin of this effect is suggested to be due to small angle scattering from the sample, which can be sufficiently suppressed by introducing a double crystal monochromator (e.g., channel-cut, Si(220), asymmetry angle $\alpha = 26°$) in the dispersive set-up [16].

In addition to the established TR-XAS set-ups, the feasibility of performing "ultra-fast" TR-XAS experiments in the femto second range using the brilliant synchrotron radiation provided by potential forth generation sources has been evaluated in several recent publications [17, 18, 19].

3. *IN-SITU* CELLS FOR TR-XAS STUDIES

A variety of flow-through cells or batch reactors can be used for *in-situ* absorption studies with X-ray photons in the energy range from 2.5 keV to 30 keV. Window materials (such as Kapton, aluminum or Beryllium foil) and gas atmospheres (e.g., $<$ 1 bar to 50 bar) can be chosen to suit the *in-situ* experiment without losing too much X-ray beam intensity, because of the absorption of photons in the *in-situ* catalysis set-up used. In principal, the large variety of *in-situ* cell designed for XAS investigations of systems under reaction conditions can also be used for TR-XAS measurements [20]. However, the application of the DXAS set-up requires improved sample homogeneity compared to the conventional scanning monochromator in order to obtain undistorted data. Hence, on one hand, DXAS studies using capillary reactors, for instance, which have been proven to be well-suited for TR studies in the QEXAFS mode, suffer from this experimental constrain. On the other hand, *in-situ* cells that permit studying chemical reactions in solutions can be successfully employed using stopped-flow techniques to perform time-resolved investigations [21, 22, 23]. *In-situ* cells that are designed for fluorescence yield measurements are restricted to the QEXAFS mode.

The following *in-situ* XAS experiments were conducted in a flow-reactor [24] on 5 mm self-supporting pellets at atmospheric pressure. The two-fold advantage of this set-up is the very small volume and the fact that the reactor can be used with both the DXAS set-up and the QEXAFS set-up. Hence, by using the same experimental cell, time-resolved DXAS data under rapidly changing conditions can be obtained (time-resolution better than 1 s), as well as high quality

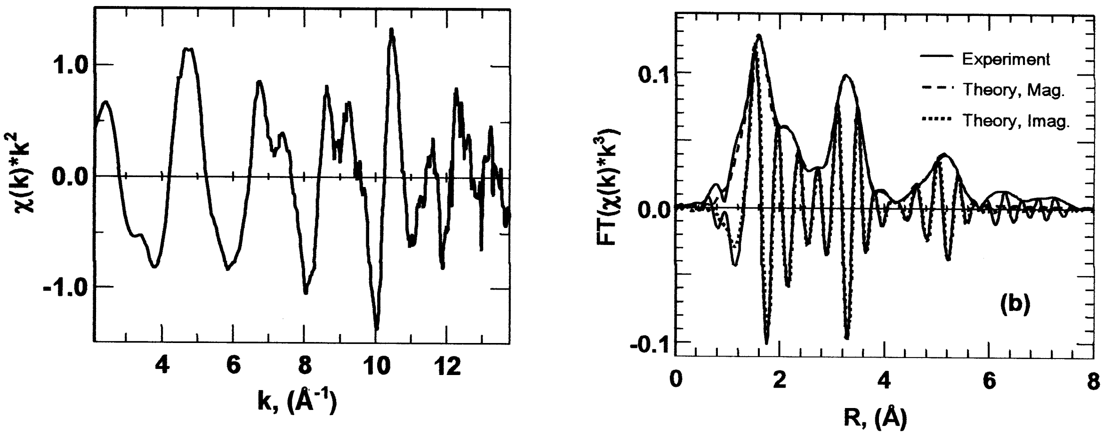

Figure 2. (Left) Experimental $\chi(k)$ of molybdenum dioxide measured in the energy-dispersive mode in 30 s. (Right) Experimental and theoretical Fourier transformed $\chi(k)$ of MoO_2. Theoretical phases and amplitudes calculated for a monoclinic MoO_2 structure were used in the refinement.

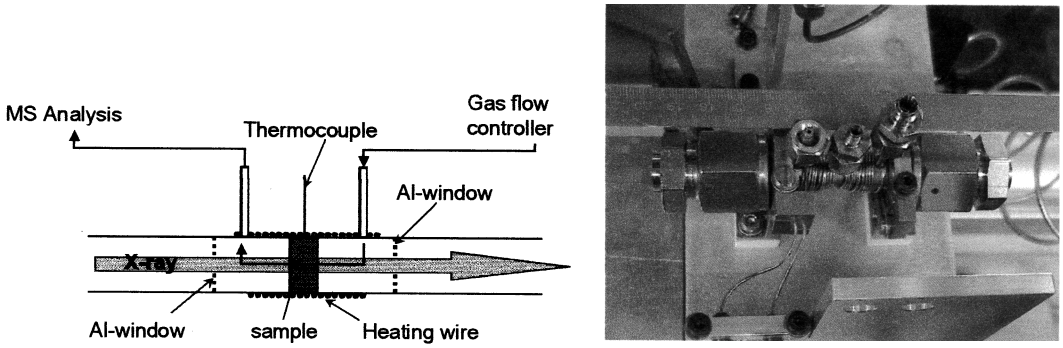

Figure 3. Schematic set-up (left) and photograph (right) of an *in-situ* cell for time-resolved XAS studies in transmission geometry using both the DXAS and the QEXAFS set-up.

EXAFS data in the conventional scanning mode or the QEXAFS mode (time-resolution of ~ 1 min). Kinetic data obtained on the quantitative reduction and re-oxidation with hydrogen, propene and oxygen, respectively (see below), confirm the suitability of a pellet reactor for investigating these processes without the problem of mass transport limitations. Temperature and reactant mass flow can be controlled with an *Eurotherm* PID temperature controller and *Bronkhorst* mass flow controllers, respectively. The product composition at the *in-situ* cell gas outlet is continuously monitored using a mass spectrometer in mass scan mode (QMS 200 from *Pfeiffer*). Continuous control of the reactant gas atmosphere is crucial for *in-situ* studies in heterogeneous catalysis when bulk structural changes are to be correlated to catalytic performance. Absolute temperature measurements were calibrated using reference compounds with tabulated phase transition temperatures (i.e., $RbNO_3$, Ag_2SO_4). Hence, transition temperatures during thermal decomposition experiments can be compared with the results of other complementary techniques.

4. ANALYSIS OF XAS DATA FROM TIME-RESOLVED EXPERIMENTS

In addition to procedures needed for conventional XAFS data analysis, time-resolved experiments require a number of features for data treatment.

Calculation of DXAS Spectra For conventional transmission, XAS measurements of the intensity of the incoming X-ray beam for each photon energy step are collected simultaneously before (I_0) and after the sample (I_1). Conversely, for every energy-dispersive XAS measurement, the I_0 signal (without a sample), the dark current of the detector, and a reference sample (I_R), most often a metal foil, have to be measured at the beginning ($I_{0,1}$) and end ($I_{0,2}$) of each experiment. Afterward, the sample under investigation (e.g., a catalyst in an *in-situ* catalysis cell) is placed into the focal point of the bent monochromator, and successive absorption signals ($I_{1,n}$) are recorded in pre-determined time intervals. In order to calculate the successive XAS spectra measured, an appropriate I_0 for every absorption signal $I_{1,n}$ needs to be calculated from a interpolation between $I_{0,1}$ and $I_{0,2}$. Using the first I_0 for all spectra may result in glitches in the absorption signal becoming more pronounced because of the current and intensity decay of the storage ring with time. On one hand, during data collection, no further movement of the spectrometer components is required, which is an advantage of the DXAS set-up compared to the conventional XAS set-up. However, on the other hand, an extremely stable beamline providing a slow and monotonous intensity decrease with time is essential for reliable DXAS measurements.

Energy Calibration of DXAS Spectra Before the DXAS spectra, which were read-out and stored during the TR experiment as a function of the photo diode number, can be further analyzed, an energy calibration needs to be performed. For that a polynomial has to be calculated representing the energy-position correlation on the detector and converting the measured absorption spectra from photo diode number to photon energy. More often than not, a deviation from a linear relationship is observed, requiring a higher-order polynomial. Using software codes that are particularly designed for the analysis of DXAS data, the coefficients of the calibration polynomial can be determined from a computer-aided comparison of the measured reference metal foil with a metal foil spectrum obtained at a conventional XAS beamline. In general, at the beginning of the calibration procedure, the software determines the edge position and suitable starting values for the polynomial coefficients. For that, the extremes of the EXAFS oscillations for both spectra are determined and a second order polynomial is refined to these extremes. A tentative absorption spectrum is computed from the DXAS reference data and superimposed on the conventional reference spectrum. In the following procedure, the coefficients of the polynomial are changed step-by-step until a satisfying match between the two reference spectra is achieved. During this refinement, the edge position has to be kept constant and the zero order of the polynomial is corrected according to the changes in the higher orders.

Automated Data Reduction Capabilities to handle a large number of spectra measured during one time-resolved experiment (regularly consisting of several hundred scans) are most important for the analysis of TR-XAS data. Here, the manual analysis of every single spectrum is hardly feasible, in particular, because many of the steps of the analysis have to be performed identically for each spectrum in order to obtain comparable results. Instead, automated procedures are required that can reliably apply certain data reduction steps, such as absorption edge determination, to each spectrum in the large TR-XAS data set [25]. The software, WinXAS, for instance, permits recording single data reduction steps and applying these parameters to each experimental absorption spectrum. Thereby, glitches can be removed, normalized spectra and derivatives can be calculated, and parameters such as edge position and fit results for each spectrum can be determined and saved sequentially. In addition, absorption signals can be averaged in order to achieve an improved data quality provided the reaction studied is still sufficiently time-resolved.

A TR-XAS data reduction can be performed already at an early stage of every TR experiment to obtain first results, as well as in a later, more thorough data analysis. In order to use the available beamtime as efficiently as possible, it is crucial to monitor the progress of a TR experiment by a continuous analysis of the measured XAS spectra. Inevitably, analysis software for TR-XAS data needs to be further improved with respect to numerical procedures and convenience in use, in order to enable a complete analysis with respect to all structural and kinetic information contained in the data. Compared to the large number of software packages available for conventional XAS data analysis, only a few packages offer features that are required for DXAS and QEXAS data analysis [compilations of XAS software can be found at "http://www.esrf.fr/computing/expg/subgroups/theory/xafs/xafs_software.html" or "http://ixs.iit.edu/catalog/XAFS_Programs"].

In order to reveal the unique information from time-resolved experiments under dynamic conditions not readily available from experiments under stationary conditions, several analysis features are particularly desirable for *in-situ* TR-XAS studies in heterogeneous catalysis. Quantitative phase analysis, for instance, is important for studies in heterogeneous catalysis where one frequently has to deal with more than one phase in the active or precursor state of the catalyst. Principle component analysis (PCA) permits a quantitative determination of the number of primary components in a set of experimental XANES or EXAFS spectra. Primary components refer to those components in the signal that are, in principle, sufficient to reconstruct each experimental spectrum by suitable linear combination. Secondary components refer to those that only contain noise. The objective of PCA of a set of experimental spectra is to determine how many "components" (i.e., reference spectra) are required to reconstruct the spectra within the experimental error. Provided that, first, the number of "references" and, second, potential references have been identified (e.g., by means of target transformation), a linear combination fit can be attempted in order to quantify the amount of each reference in each experimental spectrum. By performing a PCA prior to XANES fitting, no assumptions have to be made as of the number of references and the type of reference compounds used, and the fits can be performed with considerably less ambiguity. Details on PCA can be obtained from the literature [26, 27]. Recently, this approach has been successfully extended to the analysis of EXAFS data measured for various phase mixtures [28].

In addition to using the XANES region to elucidate phase composition and average valence, a detailed analysis of the EXAFS region can reveal the evolution of the short-range structure under reaction conditions. A structural analysis is not readily available from most conventional techniques to study solid-state kinetics (TG/DTA, TPR, etc.) which makes TR-XAS a powerful complementary tool to investigate the reactivity of solids. Using the most recent theoretical XAFS codes (such as the FEFF code [29]), the analysis of EXAFS data beyond the first coordination shell has become feasible. The multiple-shell XAFS fits are reliable because (i) a well-known crystallographic structure is refined with all its significant single and multiple scattering paths, i.e., results can be compared and validated with the literature, (ii) first shell distances are contained in a number of multiple-scattering paths with considerable amplitude and, hence, single-scattering distances are constrained in the refinement, (iii) absolute values of distances obtained are often less important than "trends" that are correlated to changes, for instance, in the catalytic activity. Eventually, using the quantitative phase information obtained from the analysis of the XANES region, a combination of more than one theoretical EXAFS function can be refined to one experimental spectrum. Thus, the short-range structure of individual phases in phase mixtures can be determined, which is also particularly important for studies in heterogeneous catalysis and solid-state chemistry [30]. Examples for the procedures mentioned are provided in the following.

5. APPLICATION OF TR-XAS

The majority of studies using time-resolved XAS concern (heterogeneous) catalysis research, focusing on both structure-reactivity relationships from investigating the catalyst under reaction conditions, as well as evolution of the catalyst structure under preparation conditions. The use of the two set-ups available (DXAS and QEXAFS) is equally distributed among these studies. However, only in few cases have both set-ups been used in a complementary manner or has the choice of the set-up employed been explained. TR-DXAS has been used to investigate both bulk metal or metal oxide catalysts and supported metal catalysts. Recently, TR-DXAS data collected are used for a kinetic analysis of the reactions proceeding in bulk catalysts [31, 32] and on supported catalysts [33–36], whereas, previously, TR-DXAS studies had mainly focused on elucidating reaction intermediates [37–42]. Evidently, owing to the limited quality of the DXAS data collected in the various studies, only few publications report a detailed EXAFS analysis of the catalytically active material under reaction conditions exceeding the first coordination shell. Moreover, although the set-ups employed in the studies cited would have provided a sub-second time-resolution, these studies did not fully exploit this potential and mainly used a time-resolution in the second range.

Most of the TR-XAS investigations employing the conventional double crystal monochromator set-up used the QEXAFS mode to obtain an improved time-resolution (on the average in the minute range) compared to the step-scanning mode. TR-QEXAFS studies were performed on both bulk metal and metal oxide catalysts [43, 44] and sulfidation catalysts [45–48, and supported catalysts [49–53]. Owing to the superior data quality in the studies cited compared to the TR-DXAS studies mentioned-above, a detailed structural analysis has been performed using the TR QEXAFS data collected. However, possibly because of the inferior time-resolution compared to TR DXAS investigations, only a few publications report a detailed kinetic analysis of the TR data obtained, and most studies focused on the identification of reaction intermediates.

In addition to studying a catalytically active material under dynamic reaction conditions, the structural evolution during the preparation of the active catalysts from a precursor material has been monitored by TR-XAS, employing either a DXAS spectrometer [54–61] or the QEXAFS mode at a conventional XAS beamline [62, 63]. Because a controlled thermal treatment of a precursor material permits a better tailoring of the time-resolution required, a time-resolution in the minute range was employed in many of the studies, resulting in a sufficient data quality to perform a detailed EXAFS analysis. Again, only a few of the cited studies report any kinetic analysis of the TR data obtained and, hence, most focused on elucidating reaction intermediates.

The structural evolution of solids during various solid-state reactions with no direct relation to heterogeneous catalysis constitutes the subject in the second largest part of investigations employing TR-XAS. A comparable number of studies employed DXAS or QEXAFS to monitor the evolution of phase composition and the short-range order structure of the materials during solid-gas reactions [64–67], solid-solid reactions [66–70], phase transformations [71–74], thermal treatments [75–80] and solid combustion syntheses [81]. The third largest fraction of investigations using TR-XAS falls in the area of electrochemistry, with a comparable number of studies employing DXAS [82–84], conventional QEXAFS [85] or QEXAFS in the reflection mode [86, 87]. To date, only few reports exist where TR-XAS has been used to study reactions in the liquid phase [88] or under environmentally relevant conditions [89]. Several additional short reports on the use of TR-XAS can be found in the proceedings of the biannual International Conference on X-ray Absorption Spectroscopy [90–94].

5.1. Solid-State Kinetics in Heterogeneous Catalysis—Reduction of MoO_3 with Propene

Structure-activity relationships constitute important subjects in heterogeneous catalysis research. In addition to reactions of the catalyst bulk during preparation and activation, the active phase and its surface can be influenced or even determined by the “real” structure of the underlying catalyst bulk. For metal oxide catalysts that are active in partial oxidation reactions, for instance, the nucleophilic oxygen that is incorporated into the reactant may stem from the catalyst bulk. Understanding the mechanism and the rate-determining step of the alternating reduction and re-oxidation steps (i.e., the reaction kinetics) is required to reveal the relationship between catalyst structure and reactivity, which eventually enables a rational catalyst design. Investigations of the relationships between the structure and the reactivity of a heterogeneous catalyst need to be performed *in-situ* (i.e., under reaction conditions) with simultaneous monitoring of the catalyst structure and the gas phase composition. “Post mortem” investigations of catalysts at room temperature, in air or inert atmosphere, cannot provide unambiguous correlations between the structure and the reactivity of the solid. In addition to studying a catalyst under stationary reaction conditions, investigations under dynamic conditions are essential to reveal structure-reactivity relationships. Eventually, only the capability to follow the structural response of the catalyst to rapidly changing reaction conditions (“chemical lock-in”) will result in a deeper understanding of the implication of the bulk structure of a catalyst for its catalytic reactivity.

Molybdenum trioxide, MoO_3, is an active catalyst for the oxidation of propene in the presence of gas phase dioxygen at temperatures above ~ 600 K [95]. Although it is assumed that the lattice oxygen of MoO_3 participates in the oxidation of propene, little is known about defects in the regular layer structure of MoO_3 that may form under reaction conditions, or about the structural properties and the role of these defects in partial oxidation reactions proceeding on the surface of the MoO_3 catalyst. Below, TR-XAS investigations combined with mass spectrometry elucidate the phase compositions and the short-range structural evolution of MoO_3 during reduction and temperature-programmed reaction (TPR) of propene and oxygen are described. The formation of characteristic defects in the bulk structure of MoO_3 under reaction conditions is investigated as a function of the reaction temperature and the reducing potential of the gas phase.

Experimental The molybdenum trioxide (MoO_3) used in the following chapters was prepared by thermal decomposition of ammonium heptamolybdate, $(NH_4)_6Mo_7O_{24}(4H_2O$ [96] (*Aldrich Co.*), in flowing synthetic air (RT – 773 K with 2 K/min, held for 2 h at 773 K). For *in-situ* XAS experiments, MoO_3 was mixed with boron nitride (ratio 1:4) and 37 mg of the mixture was pressed with a force of 1 ton into a 5 mm diameter self-supporting pellet. Time-resolved transmission XAS experiments were performed at the Mo K edge (19.999 keV) at beamline X1 at the *Hamburg Synchrotron Radiation Laboratory*, HASYLAB, using a Si(311) double crystal monochromator (measuring time $\sim$ 4.5 min/scan). The storage ring operated at 4.4 GeV with injection currents of 150 mA. Time-resolved DXAS experiments were carried out at the Mo K edge utilizing an energy-dispersive spectrometer (*European Synchrotron Radiation Facility*, ESRF, ID24 [97]) equipped with a curved Si(111) polychromator in a transmission mode (measuring time $\sim$ 3°s/scan). The storage ring operated at 6.0 GeV with injection currents of 90 mA in a 16-bunch mode. X-ray absorption fine structure (XAFS) analysis was performed using the software package WinXAS v2.2 [98] following recommended procedures from the literature [99] (see chapter 1). In the first example discussed here, the reduction of MoO_3 in propene and oxidation of MoO_2 in oxygen were investigated by time-resolved XAS combined with mass spectrometry [32]. Reduction and re-oxidation of MoO_{3-x} are of particular interest because they constitute the two fundamental steps of the so-called redox mechanism for partial oxidation of alkenes on molybdenum oxide catalysts. Temperature-programmed and isothermal TR-XAS and *in-situ* XRD experiments were performed not only to elucidate the phases present during the reactions and the structural evolution of the system, but also to reveal the solid-state kinetics of the processes involved. Eventually, a schematic reaction mechanism for the reduction of MoO_3 in propene was sought.

In addition to the evolution of the long-range order structure, *in-situ* XRD showed that during the reduction of MoO_3 in propene and the oxidation of MoO_2, crystalline MoO_3 and MoO_2 are the only phases detectable. The evolution of Mo K edge XAFS spectra measured during the temperature-

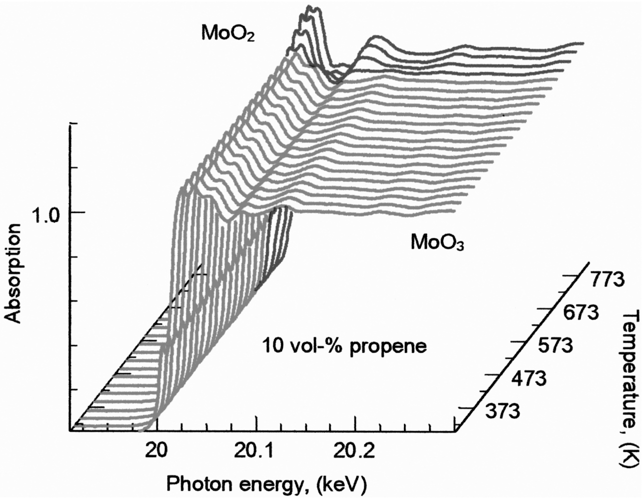

Figure 4. *In-situ* XAFS during TPR of MoO_3 in 10 vol-% propene from 300 K to 773 K at a heating rate of 5 K/min. The two most prominent phases (i.e., MoO_3 and MoO_2) are indicated.

programmed reduction of MoO_3 in 10 vol-% propene using the TR-QEXAFS technique is depicted in Figure 4. Because the temperature-programmed reaction conditions employed permit using a time-resolution in the minute range, the QEXAFS technique was chosen to obtain a sufficient data quality suitable for a detailed EXAFS analysis [32]. From Figure 4, a rapid transition between the near-edge spectra of MoO_3 and that of MoO_2 can be seen at ~ 673 K. The corresponding evolution of the Mo K edge shift and of the gas phase composition (MS ion currents of H_2O, CO_2 and acrolein) is shown in Figure 5a. For comparison, the evolution of water during the reduction of MoO_3 in 50 vol-% hydrogen is shown. An excellent agreement can be seen between the evolution of the gas phase composition (double peak in CO_2 and acrolein) and the evolution of the average molybdenum oxidation state (K edge shift). This example nicely illustrates the benefit of simultaneously monitoring the evolution of the gas phase (e.g., MS or GC) and of the structure of a catalyst (e.g., TR-XAS) to elucidate structure-reactivity relationships.

A PCA of the XANES spectra in Figure 4 revealed the presence of at least three different phases during the reduction. Target transformation of the suitable Mo oxide references showed that MoO_3, MoO_2 and $Mo_{18}O_{52}$ are suitable reference compounds for the three phases detected. A linear combination fit of the three reference spectra to the experimental XANES spectra resulted in the evolution of the three phases with temperature during reduction of MoO_3 in propene (Figure 5b). These results are complementary to *in-situ* XRD (not shown) that showed that, during the reduction of MoO_3 in propene and the oxidation of MoO_2, crystalline MoO_3 and MoO_2 are the only phases detectable. Thus, analysis of the TR-XAFS data yielded the formation of "$Mo_{18}O_{52}$" type shear-structures as a highly disordered intermediate of both the reduction of MoO_3 in propene and the oxidation of MoO_2 in oxygen.

In addition to elucidating ordered or disordered intermediate phases present during a chemical reaction, TR-XAS data are most suitable to reveal the kinetics of the reaction in the solid or the liquid phase. Figure 6 shows the extent of reduction (α) obtained from *in-situ* XAFS experiments during isothermal reduction of MoO_3 in 5 vol-% propene at 723 K, 10 vol-% propene at 673 K, and 10 vol-% propene at 698 K [32]. From the α trace at 673 K in 10 vol-% propene, a deviation from a symmetric sigmoidal trace can be seen. The acceleratory regime of the reduction at 673 K (up to $\alpha \approx 0.3$) can be described by a power rate law ($\alpha \sim t^2$), whereas the deceleratory regime of the reduction can be described by a "three dimensional diffusion" rate law ($\alpha \sim 1-(1-t^{1/2})^3$). The point of change between the two rate laws (i.e., a change in the rate-limiting step) is indicated in Figure 6. From the isothermal reduction experiments performed, it was found that the point of change between the two rate laws is approximately independent of the reaction temperature, but varies

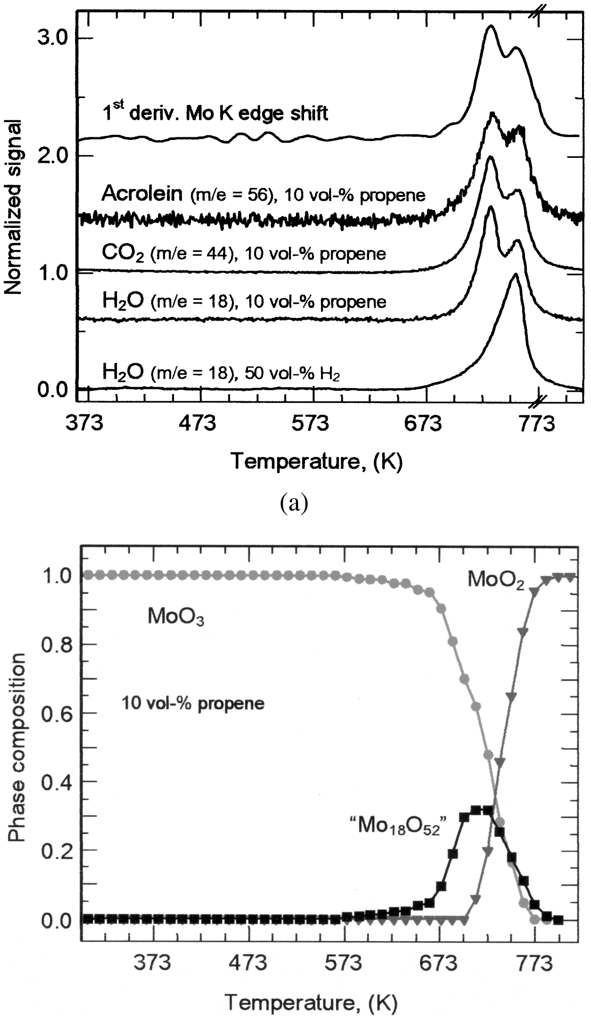

(a)

(b)

Figure 5. a) Evolution of Mo K edge shift and of the concentration of acrolein (m/e = 56), CO_2 (m/e = 44) and H_2O (m/e = 18) in the gas phase during TPR of MoO_3 in 10 vol-% propene from 300 K to 773 K (Figure 4). For comparison, the bottom trace shows the evolution of water (m/e = 18) during TPR of MoO_3 in 50 vol-% H_2. b) Evolution of phase composition (MoO_3, MoO_2 and "$Mo_{18}O_{52}$") during TPR of MoO_3 in 10 vol-% propene (Figure 4).

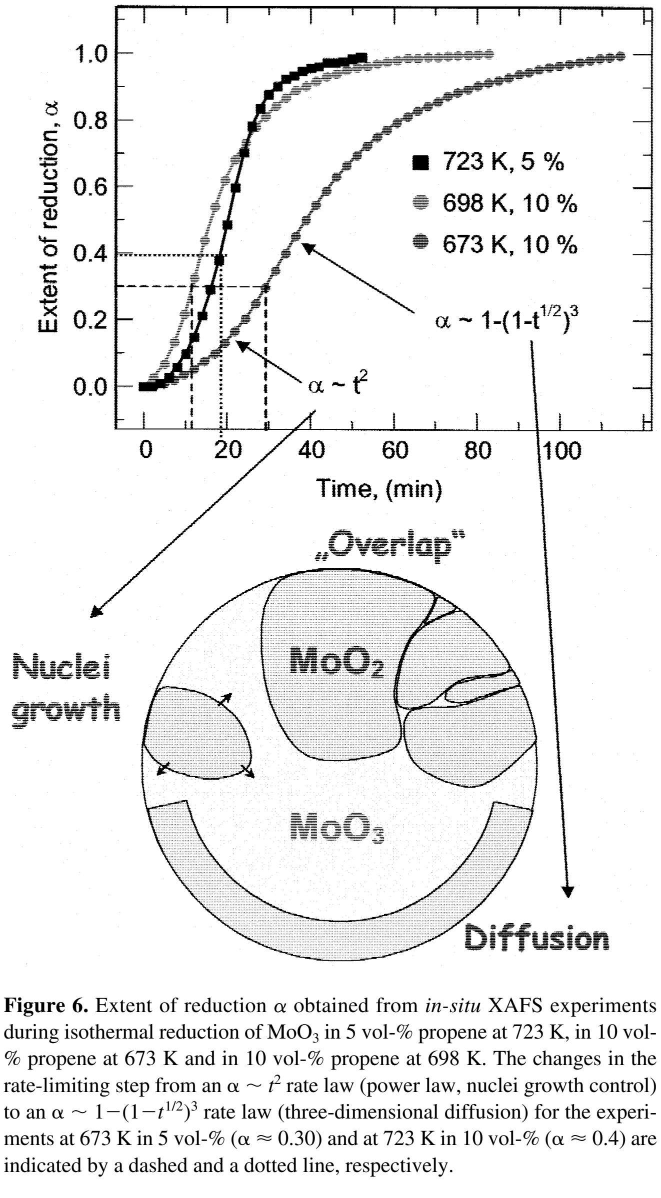

Figure 6. Extent of reduction α obtained from *in-situ* XAFS experiments during isothermal reduction of MoO_3 in 5 vol-% propene at 723 K, in 10 vol-% propene at 673 K and in 10 vol-% propene at 698 K. The changes in the rate-limiting step from an $\alpha \sim t^2$ rate law (power law, nuclei growth control) to an $\alpha \sim 1-(1-t^{1/2})^3$ rate law (three-dimensional diffusion) for the experiments at 673 K in 5 vol-% ($\alpha \approx 0.30$) and at 723 K in 10 vol-% ($\alpha \approx 0.4$) are indicated by a dashed and a dotted line, respectively.

with the reactant concentration. Apparently, the solid-state kinetics of the reduction of MoO_3 in propene exhibits a change in the rate-limiting step as a function of the extent of reduction α. With increasing α at a given temperature, transition from nuclei growth kinetics to a three-dimensional diffusion controlled regime is observed.

Ultimately, the results obtained from TR-XAS studies on the evolution of the structure of MoO_3 under reduction and oxidation conditions and the solid-state kinetics of the reduction (and possibly corroborated by complementary techniques such as *in-situ* XRD) can be combined to propose a reaction mechanism. Hence, a reaction mechanism for the reduction of MoO_3 in propene and the re-oxidation in oxygen may consist of (i) generation of oxygen vacancies at the (100) or (001) facets by reaction with propene, (ii) vacancy diffusion in the MoO_3 bulk, (iii) formation of "$Mo_{18}O_{52}$" type shear-structures in the lattice, (iv) formation and growth of MoO_2 nuclei. The mechanism is in agreement with previous reports of the propene oxidation on MoO_3 as being a structure-sensitive reaction.

5.2. Solid-State Kinetics and EXAFS Analysis of Mixtures—Oxidation of MoO_2 with Oxygen

The second example discussed here illustrates how TR-DXAS studies can be used to investigate rapid solid-state reactions and to elucidate the kinetics of the reaction and the structural evolution of the constituent phases. The oxidation of MoO_2 with oxygen at elevated temperatures was investigated by TR-XAS combined with mass spectrometry. Because at temperatures above ~ 650 K the oxidation of MoO_2 in 100 % oxygen proceeds very rapidly (at 773 K in less than one minute to completion), the DXAS technique was required to have sufficient time-resolution for studying this rapid solid-gas reaction [30]. Furthermore, this example illustrates that DXAS data can be used for a detailed EXAFS analysis. This holds not only for pure phases but also for phase mixtures, for which an analysis procedure is described below using both the XANES and EXAFS information available.

A series of Mo K near-edge (XANES) spectra was measured over a period of 10 min (2.8 s per spectrum) during oxidation of MoO_2 at various temperatures. A quantitative phase composition was obtained from a PCA of the near-edge spectra. Figure 7 shows the evolution of the extent of oxidation of MoO_2 to MoO_3 (α, defined as the fraction of MoO_3 formed) in the temperature range from 623 K to 798 K in 100 % oxygen. In the temperature range from 648 K to 798 K, the corresponding α curves exhibit a linear increase in MoO_3 concentration within the first ~ 10 s (A and B in Figure 7). In the temperature range from 723 K to 798 K, following the initial linear increase of α, an exponential increase of α with time is found (C in Figure 7), which can be described by an Avrami-Erofeev type equation $(-[\ln(1 - \alpha)]^\wedge 1/2 = kt)$ [100]. From the half-life normalized α curves (inset in Figure 7), a change in the rate-determining step between 673 K and 723 K is visible. In the temperature range from 623 K to 673 K and following the initial linear increase of α (B in Figure 7) a power-law dependence of α on time is observed (D in Figure 7). Here α can be described by the Ginstling-Brounshtein equation $(1 - 2/3\alpha - (1 - \alpha)^\wedge 2/3 = kt)$.

Apparently, the four reaction stages that govern the rate of oxidation of MoO_2 at different reaction temperatures or with the advancing extent of oxidation (increase in α) include: (A) *mass transport*, that is, the transport of oxygen from the gas phase to the MoO_2 crystallites; (B) reactions occurring at the *boundary* between MoO_2 and MoO_3. Depending on the reaction temperature, the oxidation of MoO_2 proceeds to an extent between 0.15 and 0.5 (T between 648 K and 698 K) before a change in the rate-determining step takes place; (C) growing MoO_3 *nuclei* eventually "overlap" during the proceeding oxidation of MoO_2 which results in a decrease of the oxidation rate. For this stage, reaction rate constants can be calculated with an Avrami-Erofeev type equation; (D) *diffusion* of oxygen through a layer of MoO_3 formed around a MoO_2 crystallite during oxidation. Interestingly, the four steps, found to be rate-limiting in the oxidation of MoO_2 in the temperature range from 623 K to 798 K, constitute elementary stages in many solid state reactions. For the oxidation of MoO_2, it appears that the same reaction mechanism holds over the entire

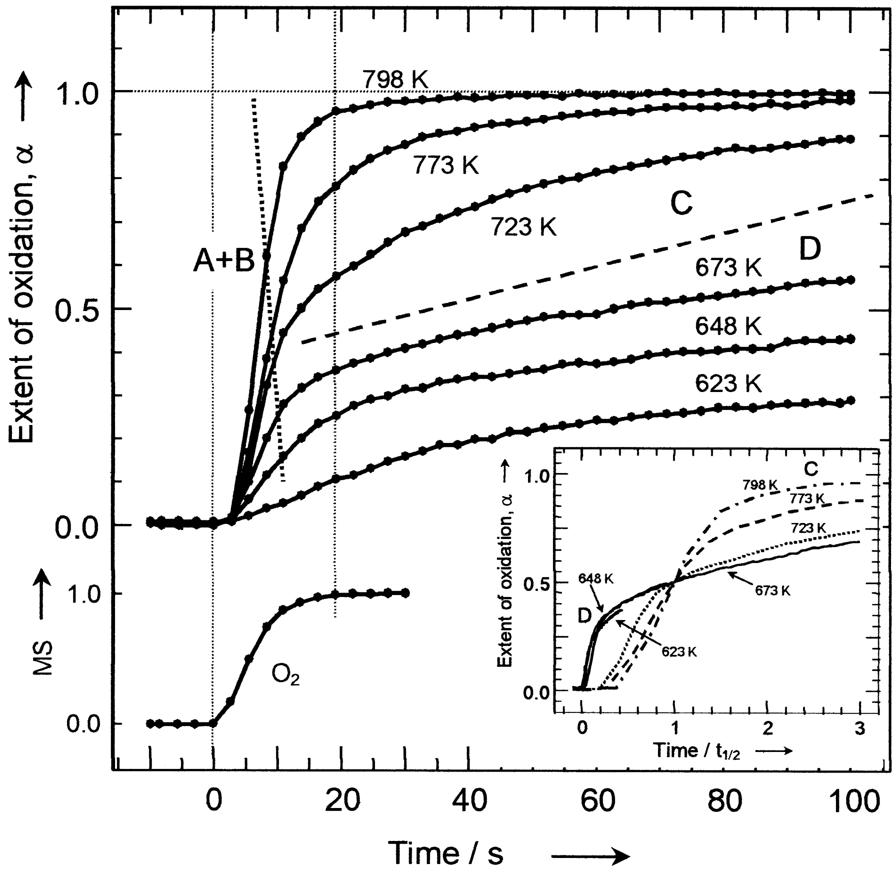

Figure 7. Evolution of the extent of oxidation (α) of MoO_2 to MoO_3 at various temperatures. (A + B) linear increase of α with time; (C) exponential increase of α; (D) power-law dependence of α on time. The heavy dotted line indicates the transition from a linear to a non-linear rate law for each α trace. The dashed line separates two regions that exhibit a different rate law. The normalized O_2 mass signal is shown to illustrate the rate of reactant transport through the *in-situ* cell. The light dotted line indicates $t = 0$ when O_2 was switched on and when the O_2 concentration reached a constant value. The inset depicts the half-life normalized evolution of α. A transition between two different rate laws can be seen.

temperature range studied and that only one or another of its "elementary" steps becomes rate-determining, depending on reaction temperature and the extent of the reaction.

In addition to a quantitative phase analysis based on the near-edge region of an X-ray absorption spectrum, the extended fine structure of the spectrum (EXAFS) can be used to reveal the structural evolution on the short-range order of the different chemical species present during the reaction. Employing state-of-the-art XAFS data analysis codes, a detailed structural analysis of the experimental EXAFS of phase mixtures is feasible. Here, the phase information obtained from XANES analysis (primary components from PCA and quantification from least-squares fits) is used to refine a sum of theoretical EXAFS functions for each phase present. In this way, structural information can be obtained to corroborate the solid-state reaction mechanism as deduced from the reaction rate law.

Selected radial distribution functions ($FT(\chi(k)*k^3)$) measured during the oxidation of MoO_2 at 673 K are depicted in Figure 8a. A transition from a MoO_2 radial distribution function (I in Figure 8a) to a MoO_3 dominated radial distribution function (VI in Figure 8a) can be seen. However, this transition does not appear to be continuous. Instead, stages (I) through (III) correspond to MoO_2 dominated radial distribution functions, where the presence of MoO_3 results only in a slight distortion, observed as a slight reduction in $FT(\chi(k))$ amplitude. Only between stages (V) and (VI) does an increase in the structural order of MoO_3 seem to take place, resulting in a MoO_3 dominated radial distribution function at stage (VI).

In Figure 8b, the evolution of the Debye temperatures of molybdenum in MoO_2 and MoO_3 during the oxidation of MoO_2 at 673 K is depicted. The Debye temperatures of molybdenum in MoO_2 and MoO_3 are obtained from a refinement of a sum of theoretical EXAFS functions of MoO_2 and MoO_3 to the experimental EXAFS functions (Figure 8a). The ratio of MoO_3 and MoO_2 was set to the ratio obtained from the PCA of the XANES spectra and was not varied in the refinement. In the analysis procedure employed, the two Debye temperatures refined represent measures of the static disorder of MoO_2 and MoO_3 in the system (isothermal conditions). For MoO_2, the continuous increase in the Debye temperature

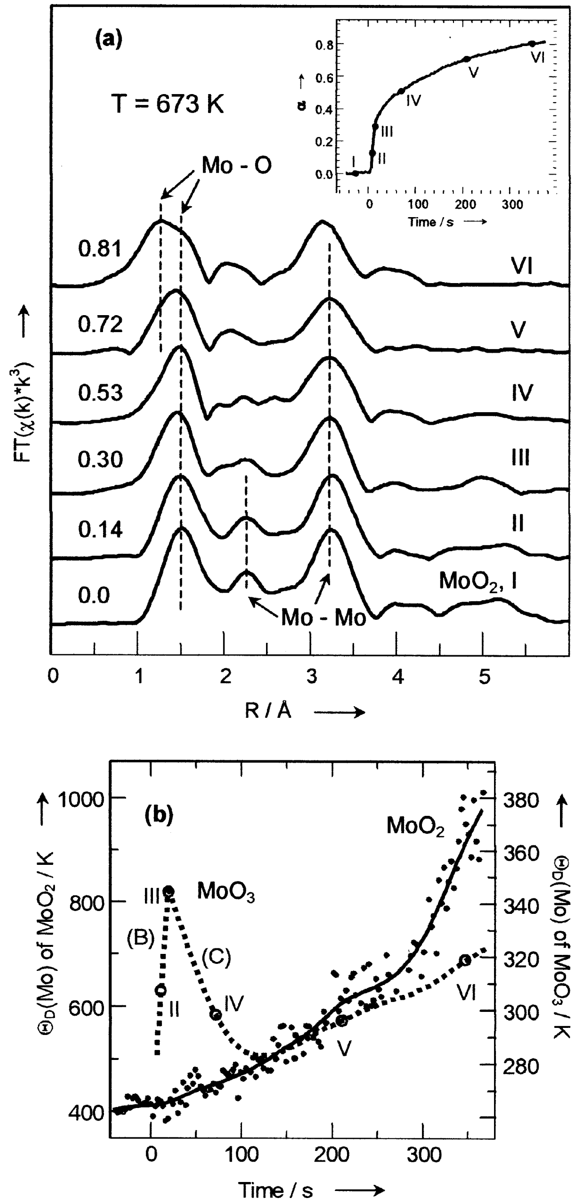

Figure 8. (a) Selected radial distribution functions (FT($\chi(k)*k^3$)) of Mo K edge spectra measured during oxidation of MoO_2 at 673 K. The inset shows the corresponding evolution of the MoO_3 phase (XANES). The fraction of MoO_3 in each FT($\chi(k)*k^3$) is given. The dashed lines indicate prominent nearest-neighbors in the radial distribution function. (b) Evolution of Debye temperatures (Θ_D(Mo)) of molybdenum in MoO_2 and MoO_3 during oxidation of MoO_2 at 673 K. For MoO_2, each point corresponds to one experimental spectrum. The solid line is drawn to guide the eye. For the Debye temperature of molybdenum in MoO_3, only a smoothed curve is shown for clarity. Stages that correspond to the FT($\chi(k)$) in a) are indicated.

indicates that Oswald ripening occurs during oxidation of MoO_2 to MoO_3. The underlying mechanism (growth of larger MoO_2 crystallites at the expense of smaller crystallites [101]) indicates the formation and growth of MoO_3 nuclei during the oxidation of MoO_2. This result corroborates the kinetic modeling based on the XANES phase analysis described above.

In contrast, for MoO_3, the evolution of the Debye temperature during the reaction exhibits three different stages (Figure 8b). Within the first 20 seconds, the increase in the Debye temperature of molybdenum in MoO_3 corresponds to the formation and initial growth of MoO_3 nuclei (B in Figure 8b, linear rate law). The subsequent decrease in the Debye temperature (C in Figure 8b) can be interpreted to originate from a MoO_3 nuclei "overlap" which leads to an increasing disorder or a recrystallization of the MoO_3 nuclei formed. Eventually, the MoO_3 crystallites formed grow and anneal, which results in an increase in the Debye temperature of molybdenum in MoO_3. In this region of α and reaction temperature, the overall rate is determined by the diffusion of oxygen through a MoO_3 product layer.

In the temperature range studied (623 K to 798 K), the same qualitative behavior in the EXAFS spectra was found. This confirms the above-mentioned conclusion that the same basic reaction mechanism for the oxidation of MoO_2 holds and that only different steps of this mechanism become rate-determining, depending on the reaction temperature and extent of reaction. In conclusion, it was deduced from the TR-XAS data presented that the oxidation of MoO_2 exhibits either a nuclei growth controlled or a diffusion controlled kinetics dependent on the reaction temperature.

5.3. Implication of the "Real" Structure of a Catalyst for Structure-Reactivity Relationships

In the third example presented here, the evolution of characteristic defects in the bulk structure of MoO_3 under propene oxidation conditions was investigated using TR-XAS combined with mass spectrometry [31]. This example will illustrate how the "real" bulk structure of a heterogeneous catalyst under reaction conditions (i.e., type and amount of defects compared to the "ideal" crystallographic structure) can be elucidated even though the data measured is clearly dominated by the "ideal" crystallographic bulk structure of the catalyst. More often than not, it is much easier to describe the "ideal" structure of a catalyst and possibly miss or ignore the small deviations thereof that constitute the defect-rich "real" structure of the catalyst. However, particularly in heterogeneous catalysis research, reliable structure-reactivity relationships depend on a detailed knowledge of both the "ideal" and the "real"structure of the catalyst. TR-XAS data measured under dynamic conditions yields trends in the various structural parameters that may be small in amplitude, but can be much more reliably interpreted than individual spectra measured under stationary conditions.

Under the reaction conditions employed (273 K to 773 K and propene to oxygen ratio from 1:1 to 1:5), MoO_3 remains the only crystalline phase detected by XRD. The onset temperature for the temperature-programmed reaction of propene and oxygen in the presence of MoO_3 coincides with the onset of the reduction of MoO_3 in He, H_2 or propene ($\sim$ 620 K). Apparently, the weakening of Mo — O bonds in MoO_3, a sufficient mobility of oxygen ions and the formation of defects are essential for the reduction of MoO_3 and for the material to function as a heterogeneous catalyst. Under propene oxidation reaction conditions, MoO_3 exhibits a slightly reduced average valence (Figure 9), which, according to the conventional redox mechanism, has to be attributed to different rates for the reduction and the re-oxidation of the molybdenum tri-

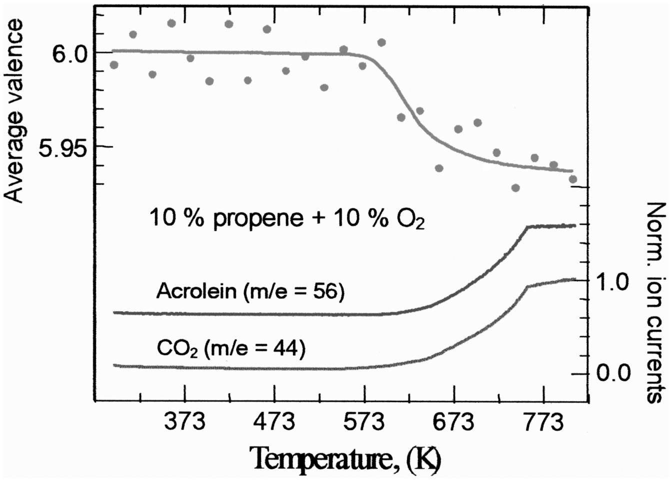

Figure 9. Evolution of average valence of MoO_3 during temperature-programmed reaction of propene and oxygen in the presence of MoO_3 (10 % O_2 and 10 % propene in He) (300 – 773 K, 5 K/min, held at 773 K) together with the evolution of the corresponding gas phase composition (CO_2 (m/e = 44) and acrolein (m/e = 56)).

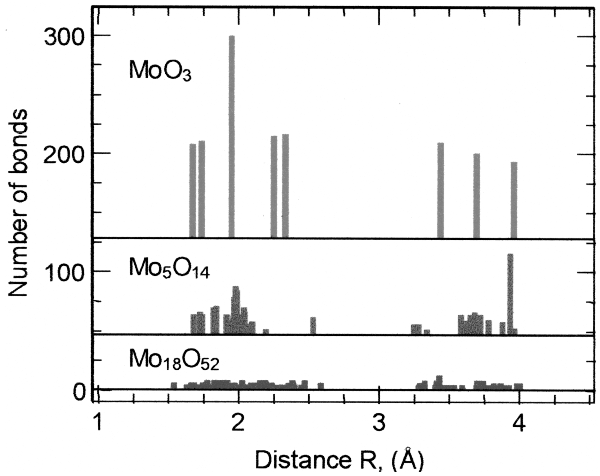

Figure 10. Comparison of radial distribution functions of MoO_3, Mo_5O_{14} and $Mo_{18}O_{52}$ calculated for cluster sizes of ~ 10 Å in both structures (~330 atoms, ~670 Mo—O and Mo—Mo bonds).

oxide [95]. Because molybdenum is known to form a number of well-defined suboxides with average valences between 6.0 (MoO_3) and 4.0 (MoO_2) (i.e., $Mo_{18}O_{52}$, $Mo_{17}O_{47}$, Mo_9O_{26}, Mo_8O_{23}, Mo_5O_{14}, Mo_4O_{11}), it has been speculated that one of these suboxides constitutes the active phase in a molybdenum oxide partial oxidation catalyst. Thus, stoichiometric reduction and oxidation of various molybdenum oxides have been studied extensively in the past, with various attempts to correlate the observations made with the catalytic behavior of the materials investigated [95]. Those studies have proven extremely valuable to elucidate the evolution of the phase composition and the bulk structure during reduction and oxidation of molybdenum oxides, and to determine the solid-state kinetics of these reactions. However, little is known about the evolution of the bulk structure of MoO_3 and the formation of defects under catalytic reaction conditions.

Although a PCA of the XANES spectra corresponding to Figure 10 did not identify a sufficiently ordered second phase, it may be legitimate to assume that "$Mo_{18}O_{52}$" type shear-structural defects are formed during the partial reduction of MoO_3 under reaction conditions. The amount of "$Mo_{18}O_{52}$" type defects formed, however, cannot readily be estimated from the Fourier transform of the Mo K edge XAFS measured under reaction conditions. A comparison of the radial distribution functions of MoO_3 and $Mo_{18}O_{52}$ for a 1 nm cluster (Figure 10) indicates that, because of the large number of slightly different distances in the structure of $Mo_{18}O_{52}$, the magnitude of the Fourier transform of $Mo_{18}O_{52}$ is considerably smaller than that of MoO_3. Hence, even major fractions of $Mo_{18}O_{52}$ in MoO_3 may be hardly noticeable from changes in the MoO_3 Fourier transform. Thus, the Mo K XAFS spectra of MoO_3 under reaction conditions correspond largely to that of pure defect-free MoO_3 at elevated temperature. The considerable number of defects in the MoO_3 structure (~ 25 % as estimated from the average Mo valence) is only accessible from their second order influence on the structural parameters as obtained from a XAFS refinement of a MoO_3 model structure to the spectra of MoO_3 under reaction conditions (Figure 11).

Simulating the effect of the presence of "$Mo_{18}O_{52}$" in MoO_3 by calculating XAFS functions that correspond to mixtures of these two oxides resulted in characteristic deviations in the XAFS fit parameters obtained for MoO_3 (i.e., increase in Debye temperatures (Figure 12a) and increase and decrease in Mo — O distances in the 1st coordination shell). For the experimental spectra measured under reaction conditions at temperatures below ~620 K, the evolution of the XAFS fit parameters is dominated by the regular effect of the increasing reaction temperature (i.e., decreasing Debye temperatures (Figure 12b) and slightly increasing Mo — O distances). However, at temperatures above ~620 K, the oxygen Debye temperatures increase drastically, while the Mo — O distances in the 1st coordination shell exhibit a characteristic pattern of increasing and decreasing distances. The deviations observed in the XAFS fit parameters obtained for MoO_3

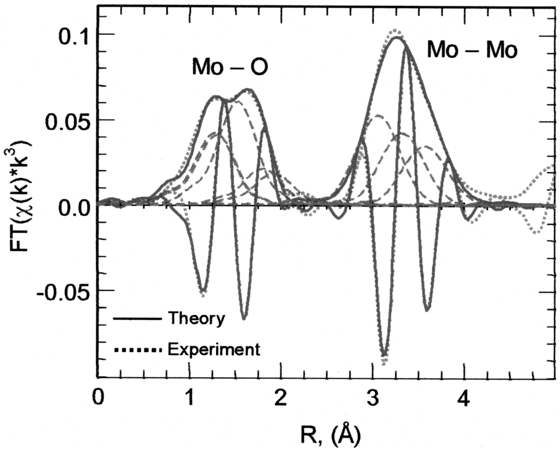

Figure 11. XAFS refinement of a theoretical Mo K edge $\chi(k)$ (solid) to an experimental Fourier transformed $\chi(k)$ of MoO_3 (dotted). The main Mo — O and Mo — Mo single-scattering paths are indicated (dashed).

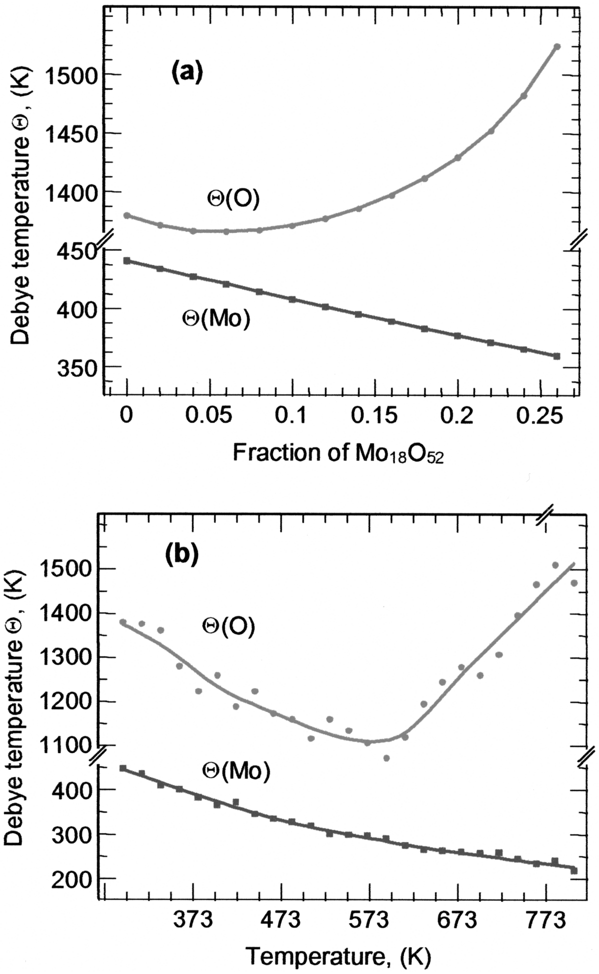

Figure 12. Evolution of Debye temperatures of molybdenum and oxygen backscatterers in the structure of MoO_3 obtained from a XAFS refinement (a) as a function of the concentration of $Mo_{18}O_{52}$ in the mixtures of MoO_3 and $Mo_{18}O_{52}$ and (b) during temperature-programmed reaction of propene and oxygen in the presence of MoO_3 (10 % O_2 and 10 % propene in He) (300 – 773 K, 5 K/min, held at 773 K).

under reaction conditions at temperatures above ~620 K are similar to those obtained for the analysis of the mixtures of MoO_3 and $Mo_{18}O_{52}$. Therefore, the XAFS analysis of the Mo K edge spectra measured under reaction conditions corroborates the formation of "$Mo_{18}O_{52}$" type defects in the layer structure of MoO_3 during oxidation of propene at temperatures below 720 K. The analysis presented depends on the reliability of small trends in structural parameters obtained from TR-XAS data and is not readily available from XAS data measured under stationary conditions.

Evidently, the catalytically active molybdenum oxide phase under partial oxidation conditions at temperatures below 720 K does not correspond to the original MoO_3 possessing the undisturbed ideal layer structure of orthorhombic α-MoO_3. Instead, at these temperatures, the catalytically active phase, which is partially reduced and possesses a large amount of "$Mo_{18}O_{52}$" type defects (crystallographic-shear structures) in the layer structure of MoO_3, develops under reaction conditions. The results presented clearly show the necessity and the large potential of bulk structural investigations of heterogeneous catalysts under reaction conditions. Evidently, the bulk structure and particularly the type and amount of defects in the material ("real" structure) considerably affect the catalytic properties. Hence, in order to rationally design a most active heterogeneous catalyst, both the structure and reactions of the surface and structure defects and reactions of the bulk need to be known in detail and carefully considered.

6. OUTLOOK

The examples presented in this chapter clearly demonstrate the potential of TR-XAS investigations to extend the suitability of XAS for *in-situ* studies in heterogeneous catalysis to investigations under dynamic conditions. XAS experiments under stationary conditions reveal the structure of the working catalyst, however, correlations between the structure of the catalyst and its catalytic properties can only be elucidated from monitoring the structural response of the catalyst to (rapidly or even periodically) changing reaction conditions ("chemical lock-in"). The examples presented illustrate that the available experimental TR-XAS set-ups are very much suitable to accomplish this task, although each has its characteristic advantages and disadvantages.

Although many studies have been performed using either the QEXAFS or the DXAS technique for TR-XAS measurements, little use has been made of combining the specific advantages of the two set-ups for time-resolved XAS studies. On one hand, TR-XAS investigations that require the best time-resolution available (such as isothermal reactions or rapid decompositions with half-lives in the order of one minute) should be performed at an energy-dispersive XAFS station, taking full advantage of the time-resolution, even at the expense of data quality. On the other hand, TR-XAS studies of processes with half-lives in the order of 30 min may be performed in the QEXAFS mode, taking advantage of the increased EXAFS data quality for a detailed structural analysis. The objective needs to be to properly time-resolve the process under investigation and to avoid time-averaging as much as possible, while measuring XAFS spectra with the best data quality available.

Although the experiments shown demonstrate the wealth of kinetic and structural data that can be obtained from TR-XAS studies, application of *in-situ* XAS combined with complementary techniques provide unique and detailed information. This does not only refer to the most elegant way of using XAS simultaneously with other methods (e.g., XRD [102, 103, 104, 105]), but also to simply substantiate results obtained from *in-situ* XAFS studies with those obtained from complementary *in-situ* studies under similar experimental conditions (e.g., laboratory techniques such as *in-situ* XRD, Raman, TG/DTA, etc.). More often than not, a detailed XAFS analysis is only possible by using all additional data (phases, valence and structure) about the system under investigation. Furthermore, the analysis of TR-XAS data should aim at extracting as much information from the XANES part and the EXAFS part of a XAS spectrum as possible.

Eventually, for time-resolved studies on solid-solid or solid-gas reactions in heterogeneous catalysis, a lower limit for the required time-resolution exists, because of the required mass transport to the catalyst surface. In flow reactors, the gas phase transport to the catalyst surface, after rapidly changing the gas atmosphere, usually amounts to several seconds. Hence, a time resolution in the range of ∼ 100 ms should be absolutely sufficient to resolve the changes in the bulk structure induced by the variation in gas composition or reaction temperature.

More important than pushing the time-resolution into the microsecond range is measuring X-ray absorption data of superior quality. Therefore, to evaluate data quality and time-resolution of a particular experimental station, "real" systems under *in-situ* conditions should be compared (e.g., 3d and 4d metal oxides at elevated temperature measured to k equal to 16 A^{-1} rather than metal foils). It must be kept in mind that kinetic data can also be obtained from complementary methods such as TG/DTA, TPR or TPRS, whereas complementary *in-situ* techniques (e.g., XRD, Raman, IR, UV-VIS) can provide structural and/or valence information under reaction conditions. However, the capability of TR-XAS to reveal *quantitative phase composition and average valence* together with the evolution of the *local structure* of a system under varying (reaction) conditions, combined with a time-resolution of 100 ms, shall be a very powerful tool for kinetic studies in solid-state chemistry and heterogeneous catalysis.

REFERENCES

1. Dent, A. J., *Top. Catal.*, 18(1–2), 27–35 (2002).
2. Ressler, T., Wienold, J., Jentoft, R. E., Neisius, T., Gunter, M. M., *Top. Catal.*, 18(1–2), 45–52 (2002).
3. Grunwaldt, J. D., Clausen, B. S., *Top. Catal.*, 18(1–2), 37–43 (2002).
4. Newton, M. A., Dent, A. J., Evans, J., *Chem. Soc. Rev.*, 31, 83–95 (2002).
5. Shido, T., Prins, R., *Curr. Opin. Solid State Mat. Sci.*, 3, 330–335 (1998).
6. Frahm, R., *Nucl. Instrum. Meth. A*, 270, 578 (1988).
7. Frahm, R., *Rev. Sci. Instrum.* 60, 7, 2515 (1989).
8. Richwin, M., Zaeper, R., Lutzenkirchen-Hecht, D., Frahm, R., *Rev. Sci. Instrum.*, 73, 1668–1670 (2002).
9. Kappen, P., Troger, L., Materlik, G., Reckleben, C., Hansen, K., Grunwaldt, J. D., Clausen, B. S., *J. Synchrot. Radiat.*, 9, 246–253 (2002).
10. Zaeper, R., Richwin, M., Wollmann, R., Lutzenkirchen-Hecht, D., Frahm, R., *Nucl. Instrum. Methods Phys. Res. A*, 467, 994–997 (2001).
11. Als-Nielsen, J., Grubel, G., Clausen, B. S., *Nucl. Instrum. Meth. Phys. Res. B.*, 97, 522–525 (1995).
12. Hagelstein, M., San Miguel, A., Fontaine, A., Goulon, J., *J. de Physique IV* 7, C2-303 (1997).
13. Kaminaga, U., Matsushita, T., Kohra, K., *Jap. J. Appl. Phys.* 20, 5, 355 (1981).
14. Koch, A., Hagelstein, M., San Miguel, A., Fontaine, A., Ressler, T., *SPIE*, 2461, 85 (1995).
15. Hagelstein, M., Ferrero, C., Hatje, U., Ressler, T., Metz, W., *J. Synchrot. Radiat.*, 2, 174–180 (1995).
16. Hagelstein, M., Lienert, U., Ressler, T., San Miguel, A., Freund, A., Cunis, S., Schulze, C., Fontaine, A., Hodeau, J.-L., *J. Synchrot. Radiat.*, 5, 753 (1998).
17. Bressler, C., Saes, M., Chergui, M., Grolimund, D., Abela, R., Pattison, P., *J. Chem. Phys.*, 116, 2955–2966 (2002).
18. Chen, L. X., *J. Electron Spectrosc. Relat. Phenom.*, 119, 161–174 (2001).
19. Tomov, I. V., Oulianov, D. A., Chen, P. L., Rentzepis, P. M., *J. Phys. Chem. B*, 103, 7081–7091 (1999).
20. Clausen, B. S., Steffensen, G., Fabius, B., Villadsen, J., Feidenhans'l, R., Topsoe, H., *J. Catal.*, 132, 524 (1991).
21. Inada, Y., Hayashi, H., Funahashi, S., Nomura, M., *Rev. Sci. Instrum.*, 68, 2973–2977 (1997).
22. Scheuring, E. M., Clavin, W., Wirt, M. D., Miller, L. M., Fischetti, R. F., Lu, Y., Mahoney, N., Xie, A. H., Wu, J. J., Chance, M. R., *J. Phys. Chem.*, 100, 3344–3348 (1996).
23. Thiel, D. J., Livins, P., Stern, E. A., Lewis, A., *Nature*, 362, 40–43 (1993).
24. Designed by M. Hagelstein, T. Neisius, *et al.*, ESRF, in a collaborative effort with the Fritz-Haber-Institut, Berlin, Germany.
25. Ressler, T., *J. Synchrot. Radiat.*, 5, 118–122 (1998).
26. Malinowski, E. R., Howery, D. G., *Factor Analysis in Chemistry*, John Wiley and Sons, New York, 1980.
27. Ressler, T., Wong, J., Roos, J., Smith, I. L., *Environ. Science & Techn.* 34, 950 (2000).
28. Frenkel, A. I., Kleifeld, O., Wasserman, S. R., Sagi, I., *J. Chem. Phys.*, 116, 9449–9456 (2002).
29. Rehr, J. J., Booth, C. H., Bridges, F., Zabinsky, S. I., *Phys. Rev. B*, 49, 12347 (1994).
30. Ressler, T., Wienold, J., Jentoft, R E., Timpe, O., Neisius, T., *Solid State Commun.*, 119, 169–174 (2001).
31. Ressler, T., Wienold, J., Jentoft, R. E., Girgsdies, F., *Eur. J. Inorg. Chem.* accepted.
32. Ressler, T., Jentoft, R. E., Wienold, J., Neisius, T., *J. Catal.*, 210, 67–83 (2002).
33. Evans, J., Newton, M. A., *J. Mol. Catal. A: Chem.*, 182 (1), 351–357 (2002).
34. Evans, J., O'Neill, L., Kambhampati, V. L., Rayner, G., Turin, S., Genge, A., Dent, A. J., Neisius, T., *J. Chem. Soc.-Dalton Trans.*, 10, 2207–2212 (2002).
35. Newton, M. A., Burnaby, D. G., Dent, A. J., Diaz-Moreno, S., Evans, J., Fiddy, S. G., Neisius, T., Turin, S., *J. Chem. Phys. B*, 106, 4214–4222 (2002).
36. Newton, M. A., Burnaby, D. G., Dent, A. J., Diaz-Moreno, S., Evans, J., Fiddy, S. G., Neisius, T., Pascarelli, S., Turin, S., *J. Chem. Phys. A*, 105, 5965–5970 (2001).
37. Lamberti, C., Prestipino, C., Bonino, F., Capello, L., Bordiga, S., Spoto, G., Zecchina, A., Moreno, S. D., Cremaschi, B., Garilli, M., Marsella, A., Carmello, D., Vidotto, S., Leofanti, G., *Angew. Chem.-Int. Edit.*, 41(13), 2341–2344 (2002).
38. Bottger, I., Schedel-Niedrig, T., Timpe, O., Gottschall, R., Havecker, M., Ressler, T., Schlogl, R., *Chem.-Eur. J.*, 6, 1870–1876 (2000).
39. Ressler, T., Timpe, O., Neisius, T., Find, J., Mestl, G., Dieterle, M., Schlogl, R., *J. Catal.*, 191, 75–85 (2000).
40. Hagelstein, M., Hatje, U., Forster, H., Ressler, T., Metz, W., *Studies in Surface Science and Catalysis*, 84, 1217–1222 (1994).
41. Sankar, G., Thomas, J. M., Waller, D., Couves, J. W., Catlow, C. R. A., Greaves, G. N., *J. Phys. Chem.*, 96, 7485–7489 (1992).
42. Ressler, T., Hagelstein, M., Hatje, U., Metz, W., *J. Phys. Chem. B*, 101, 34, 6680 (1997).
43. Gunter, M. M., Ressler, T., Jentoft, R. E., Bems, B., *J. Catal.*, 203, 133–149 (2001).
44. Reitz, T. L., Lee, P. L., Czaplewski, K. F., Lang, J. C., Popp, K. E., Kung, H. H., *J. Catal.*, 199, 193–201 (2001).
45. Sun, M. Y., Burgi, T., Cattaneo, R., van Langeveld, D., Prins, R., *J. Catal.*, 201, 258–269 (2001).
46. Geantet, C., Soldo, Y., Glasson, C., Matsubayashi, N., Lacroix, M., Proux, O., Ulrich, O., Hazemann, J. L., *Catal. Lett.*, 73, 95–98 (2001).
47. Cattaneo, R., Rota, F., Prins, R., *J. Catal.*, 199, 318–328 (2001).
48. Cattaneo, R., Weber, T., Shido, T., Prins, R., *J. Catal.*, 191, 225–236 (2000).
49. Oudenhuijzen, M. K., Kooyman, P. J., Tappel, B., van Bokhoven, J. A., Koningsberger, D. C., J. Catal., 205, 135–146 (2002).
50. Grunwaldt, J. D., Kappen, P., Basini, L., Clausen, B. S., *Catal. Lett.*, 78, 13–21 (2002).

51. Grunwaldt, J. D., Molenbroek, A. M., Topsoe, N. Y., Topsoe, H., Clausen, B. S., *J. Catal.*, 194, 452–460 (2000).
52. Ovesen, C. V., Clausen, B. S., Schiotz, J., Stoltze, P., Topsoe, H., Norskov, J. K., *J. Catal.*, 168, 133–142 (1997).
53. Clausen, B. S., Grabaek, L., Steffensen, G., Hansen, P. L., Topsoe, H., *Catal. Lett.*, 20, 23–36 (1993).
54. Shido, T., Yamaguchi, A., Inada, Y., Asakura, K., Nomura, M., Iwasawa, Y., *Top. Catal.*, 18(1–2), 53–58 (2002).
55. Yamaguchi, A., Suzuki, A., Shido, T., Inada, Y., Asakura, K., Nomura, M., Iwasawa, Y., *J. Phys. Chem. B*, 106, 2415–2422 (2002).
56. Fiddy, S. G., Newton, M. A., Campbell, T., Dent, A. J., Harvey, I., Salvini, G., Turin, S., Evans, J., *Phys. Chem. Chem. Phys.*, 4, 827–834 (2002).
57. Yamaguchi, A., Inada, Y., Shido, T., Asakura, K., Nomura, M., Iwasawa, Y., *Catal. Lett.*, 68, 139–145 (2000).
58. Hatje, U., Ressler, T., Petersen, S., Forster, H., *J. Phys. IV*, 4, 141–144 (1994).
59. Sankar, G., Wright, P. A., Natarajan, S., Thomas, J. M., Greaves, G. N., Dent, A. J., Dobson, B. R., Ramsdale, C. A., Jones, R. H., *J. Phys. Chem.*, 97, 9550–9554 (1993).
60. Thomas, J. M., Greaves, G. N., Sankar, G., Wright, P. A., Chen, J., Dent, A. J., Marchese, L., *Angew. Chemie Intl. Ed.*, 33, 1871 (1993).
61. Couves, J. W., Catlow, C. R. A., Greaves, G. N., Thomas, J. M., *J. Phys. Chem.*, 96, 7485 (1992).
62. Wienold, J., Jentoft, R. E., Ressler, T., *Eur. J. Inorg. Chem.*, accepted.
63. Cimini, F., Prins, R., *J. Phys. Chem. B*, 101, 5277–5284 (1997).
64. Rodriguez, J. A., Hanson, J. C., Frenkel, A. I., Kim, J. Y., Perez, M., *J. Am. Chem. Soc.*, 124, 346–354 (2002).
65. Ressler, T., Wienold, J., Jentoft, R. E., *Solid State Ionics* 141–142, 243–251 (2001).
66. Ressler, T., Jentoft, R. E., Wienold, J., Gunter, M. M., Timpe, O., *J. Phys. Chem. B*, 104, 6360–6370 (2000).
67. Rodriguez, J. A., Chaturvedi, S., Hanson, J. C., Brito, J. L., *J. Phys. Chem. B*, 103, 770–781 (1999).
68. Rumpf, H., Janssen, J., Modrow, H., Winkler, K., Hormes, J., *J. Solid State Chem.*, 163, 158–162 (2002).
69. Grunwaldt, J. D., Lutzenkirchen-Hecht, D., Richwin, M., Grundmann, S., Clausen, B. S., Frahm, R., *J. Phys. Chem. B*, 105, 5161–5168 (2001).
70. Chauvistre, R., Hormes, J., Sommer, K., *Kautsch. Gummi Kunstst.*, 47, 481–484 (1994).
71. Rodriguez, J. A., Hanson, J. C., Chaturvedi, S., Maiti, A., Brito, J. L., *J. Phys. Chem. B*, 112, 935–945 (2000).
72. Douillard, L., GautierSoyer, M., Duraud, J. P., Fontaine, A., Baudelet, F., *J. Phys. Chem. Solids*, 57, 495–501 (1996).
73. Dacapito, F., Boscherini, F., Buffa, F., Vlaic, G., Paschina, G., Mobilio, S., *J. Non-Cryst. Solids*, 156, 571–574 (1993).
74. Rodriguez, J. A., Chaturvedi, S., Hanson, J. C., Albornoz, A., Brito, J. L., *J. Phys. Chem. B*, 102, 1347–1355 (1998).
75. Choy, J. H., Kim, Y. I., Yoon, J. B., Choy, S. H., *J. Mater. Chem.*, 11, 1506–1513 (2001).
76. Pickup, D. M., Mountjoy, G., Holland, M. A., Wallidge, G. W., Newport, R. J., Smith, M. E., *J. Phys.-Condes. Matter*, 12, 9751–9760 (2000).
77. Walton, R. I., Hibble, S. J., *J. Mater. Chem.*, 9, 1347–1355 (1999).
78. Walton, R. I., Dent, A. J., Hibble, S. J., *Chem. Mater.*, 10, 3737–3745 (1998).
79. Hilbrandt, N., Martin, M., *Solid State Ion.*, 95, 61–64 (1997).
80. Troger, L., Hilbrandt, N., Epple, M., *J. Phys. IV*, 7, 323–324 (1997).
81. Frahm, R., Wong, J., Holt, J. B., Larson, E. M., Rupp, B., Waide, P. A., *Phys. Rev. B*, 46, 9205–9208 (1992).
82. Allen, P. G., Conradson, S. D., Wilson, M. S., Gottesfeld, S., Raistrick, I. D., Valerio, J., Lovato, M., *J. Electroanal. Chem.*, 384, 99–103 (1995).
83. Millet, P., Durand, R., Dartyge, E., Tourillon G., Fontaine, A., *J. Electrochem. Soc.*, 140, 1373–1380 (1993).
84. Guay, D., Tourillon, G., Dartyge, E., Fontaine, A., McBreen, J., Pandya, K. I., OGrady, W. E., *J. Electroanal. Chem.*, 305, 83–95 (1991).
85. Lutzenkirchen-Hecht, D., Frahm, R., *J. Phys. Chem. B*, 105, 9988–9993 (2001).
86. Hecht, D., Borthen, P., Frahm, R., Strehblow, H. H., *J. Phys. IV*, 7, 717–722 (1997).
87. Hecht, D., Frahm, R., Strehblow, H. H., *J. Phys. Chem.*, 100, 10831–10833 (1996).
88. Epple, M., Troger, L., Hilbrandt, N., *J. Chem. Soc. – Faraday Trans.*, 93, 3035–3037 (1997).
89. Villinski, J. E., O'Day, P. A., Corley, T. L., Conklin, M. H., *Environ. Sci. Technol.*, 35, 1157–1163 (2001).
90. XAFS XI Proceedings, *J. Synchrot. Radiat.*, 8(2) (2001).
91. XAFS X Proceedings, *J. Synchrot. Radiat.*, 6(5) (1999).
92. XAFS IX Proceedings, *J. Phys. IV*, 7(C2) (1997).
93. XAFS VIII Proceedings, *Physica B*, 1–4 (1995).
94. XAFS VII Proceedings, *Jpn. J. Appl. Phys.* Part 1, 32 (1993).
95. Grzybowska-Swierkosz, B., *Topics in Catalysis*, 11/12, 23–42 (2000).
96. Wienold, J., Jentoft, R. E., Ressler, T., *Eur. J. Inorg. Chem.* (2002), submitted.
97. Hagelstein, M., San Miguel, A., Fontaine, A., Goulon, J., *J. de Physique IV*, 7, C2-303 (1997).
98. Ressler, T., *J. Synch. Rad.*, 5, 118–122 (1998).
99. Koningsberger, D. C., Prins, R., *X-ray Absorption Spectroscopy, Chemical Analysis*, 92, Wiley, New York, 1988.
100. C. H. Bamford, Ed., Comprehensive Chemical Kinetics, Vol. 2, Elsevier, 1968.
101. Schmalzried, H., *Solid State Kinetics*, VCH-Verlag Weinheim, 1994.
102. Dent, A. J., Greaves, G. N., Roberts, M. A., Sankar, G., Wright, P. A., Jones, R. H., Sheehy, M., Madill, D., Catlow, C. R. A., Thomas, J. M., Rayment, T., *Nucl. Instrum. Meth. Phys. Res. B.*, 97, 20–22 (1995).
103. Thomas, J. M., Greaves, G. N., Richard, C., Catlow, C. R. A., *Nucl. Instrum. Methods Phys. Res. B*, 97, 1–10 (1995).
104. Clausen, B. S., *Catal. Today*, 39, 293–300 (1998).
105. Clausen, B. S., Graback, K., Steffensen, G., Hansen, P. L., Topsoe, H., *Catal. Lett.*, 20, 23 (1993).